Clinical & Experimental Metastasis (2019) 36:411–422
https://doi.org/10.1007/s10585-019-09979-w

RESEARCH PAPER

Identification of S100A14 as a metastasis-promoting molecule in a murine organotropic metastasis model

Takashi Sugino[1] · Naoki Ichikawa-Tomikawa[2] · Mizuko Tanaka[2] · Namiko Shishito[3] · Tomiko Miura[2] · Masato Abe[1] · Koji Muramatsu[1] · Takuma Oishi[1] · Yuko Kakuda[1] · Takuya Kawata[1] · Yasuto Akiyama[4]

Received: 24 January 2019 / Accepted: 10 June 2019 / Published online: 1 July 2019

Abstract

Cancer metastasis shows great diversity in target organs, routes and molecular mechanisms depending on the type of cancer and even on the individual patients. To identify key molecules involved in metastasis, we constructed a murine model system including multiple sublines with different organotropism and pathways of metastasis. We selected metastatic sublines from a murine mammary tumor cell line MCH66. Using this model, we extracted metastasis-related molecules by gene expression screening methods and verified their metastasis-promoting effects by gene knockdown or overexpression experiments. For the candidates promoting metastasis, we analyzed molecular functions involved in metastasis: cell growth, motility and invasive activity. We established a metastasis model including low metastatic sublines (66C8, 66LM, 66-4) and highly metastatic counterparts with various organotropism, such as to the lung (66Lu10), liver (HM-KAN5) and general organs (66HM and its clones: HM1-6 and HM1-7). The sublines basically exhibited the invasion-independent metastasis pathway characterized by endothelial cell-covered tumor emboli, whereas 66HM and HM-KAN5 showed an alternative metastasis pathway based on invasion in part and in whole, respectively. Comprehensive gene analysis extracted several molecular candidates responsible for metastasis. S100A14 was identified as one of the promissing candidates promoting lung-metastasis, which was verified by gene knockdown experiments in vivo. In addition, in vivo and in vitro functional analyses demonstrated that S100A14 enhanced scattering, motility and invasiveness of mouse tumor cells. Our model system may be adaptable to the diversity of metastasis in human cancers and useful for exploring the molecular mechanism responsible for metastasis.

Keywords Metastasis · Animal model · Gene screening · S100A14

Abbreviations

SLPI	Secretory leukocyte protease inhibitor
RAGE	Receptor for advanced glycation end products
SSH	Suppressive subtractive hybridization

Introduction

Cancer metastasis is the most serious cause of death for patients and its control is considered to be a clinical task of high priority. However, because metastasis is a diverse and complex phenomenon, understanding the mechanism and development of therapeutic methods are not progressing rapidly. The diversity of metastasis includes organotropism, routes and pathways, which vary depending on the type of cancer as well as among individual cases.

Organotropism of metastasis, a phenomenon in which some cancers tend to spread to specific organs, has been understood on the basis of two major hypotheses: "mechanical/anatomical hypothesis" and "seed and soil hypothesis". Many experimental studies on metastasis have focused on the interaction between cellular properties inherent to a cancer and the microenvironment of the target organ.

Metastasis can occur by various routes, such as "blood-borne", "lymphatic" and "disseminated". In contrast to the

Electronic supplementary material The online version of this article (https://doi.org/10.1007/s10585-019-09979-w) contains supplementary material, which is available to authorized users.

✉ Takashi Sugino
t.sugino@scchr.jp

[1] Division of Pathology, Shizuoka Cancer Center, Shizuoka 411-8777, Japan

[2] Department of Basic Pathology, Fukushima Medical University School of Medicine, Fukushima, Japan

[3] Department of Cardiology, Southern TOHOKU General Hospital, Koriyama, Japan

[4] Division of Immunotherapy, Shizuoka Cancer Center Research Institute, Shizuoka, Japan

sequential progression model, which stipulates that lymph node metastases give rise to distant metastases, a recent study demonstrated that metastases can originate from independent subclones within the primary tumor in colorectal cancer [1]. This finding suggests that there may be different cellular lineages and properties for individual routes of metastasis.

In the general concept of the metastatic process, "invasion", in which cancer cells disrupt the surrounding stroma and blood vessels, is considered to be an indispensable step. In contrast, we previously presented a mouse model of an "invasion-independent pathway" as an alternative concept of metastasis whereby cancer cells can enter the circulation without penetrating the vessel wall [2]. This pathway may exist in some human cancers, such as hepatocellular carcinoma, renal cell carcinoma and follicular thyroid carcinoma [3, 4].

At present, in vivo metastasis models remain insufficient; thus, it is essential for metastasis research to establish models that recapitulate the diversity of human cancer metastasis. We previously established a metastatic cell line, MCH66, from a mouse mammary tumor and selected a non-metastatic clone, 66C8, using single cell cloning method [5]. Furthermore, we have also selected a highly metastatic subline that exhibits lung metastases, 66Lu10, using an in vivo selection method [6]. We have performed differential screening of mRNA expression in a set of highly and low-metastatic sublines and revealed that secretory leukocyte protease inhibitor (SLPI) promotes lung metastasis via an invasion-independent pathway in mouse mammary tumor [5].

In this study, we established additional new sublines and cell clones with metastatic potential for the liver or general organs. As a results, we provided a murine model system of cancer metastasis including a variety of organotropism and pathways that are dependent or independent on an invasion step to the vascular wall. Since all of these sublines originated from a single cell line, MCH66, they are expected to have the same genetic background other than the genes involved in metastasis. Thus, the metastasis-related genes can be easily extracted by comparing sublines with different metastatic potential. Using this model system, we extracted genes common to two combinations of highly and low-metastatic sublines and identified candidate genes that promote or suppress metastasis with higher precision. As a result, we identified S100A14 as a candidate metastasis-promoting molecule. Based on this information, we conducted experimental and clinicopathological studies on human breast cancer, and we previously reported that S100A14 promotes cellular motility and invasiveness of human breast cancer cells and that upregulated expression of S100A14 is associated with poor prognosis in breast cancer patients [7].

The S100 protein family, to which S100A14 belongs, has a broad range of intracellular functions, such as cell growth, differentiation and motility, through the interaction with specific target proteins [8, 9]. S100A14 can bind to cortical actin, HER2 and the receptor for advanced glycation end products (RAGE) to affect proliferation, invasion and motility of cancer cells [7, 10, 11]. Although the correlation of S100A14 expression with cancer patient prognosis is controversial, many papers reported that the overexpression of this protein is correlated with poorer prognosis, recurrence and drug resistance in many types of cancers except in the gastrointestinal tract [7, 12–16].

We present here a murine model that is comprised of multiple sublines with varied metastasis potentials and organotropism, as well as our project for the identification of metastasis-related molecules using this model system. Furthermore, we describe a candidate molecule, S100A14, which promotes cellular motility, invasion and lung metastasis of the mouse mammary tumor.

Methods

Cell lines and cell culture

The parent mouse mammary tumor line, MCH66, and its sublines were cultured in 5% CO_2 at 37 °C and grown in complete medium, which was composed of DMEM, low glucose (WAKO, Japan) and 10% fetal bovine serum (GIBCO).

Gene expression analysis

Total RNA was extracted from subcloned cells using TRIzol RNA Isolation Reagents (Thermo Fisher Scientific, Ltd., Japan). Gene expression analyses were performed with a suppression subtractive hybridization (PCR-Select cDNA Subtraction kit, Takara Bio, Japan) (ref.) and a microarray analysis using a contract analysis with a 3D-Gene Mouse Oligo chip 24K (Toray Industries, Inc., Tokyo, Japan).

To select metastasis-related genes, we first selected top 19 genes with high expression ratio of the high-metastatic to low metastatic sublines in common in the two analyzes. Then, expression levels of the genes in 66C8, 66LM, 66HM, Lu1 and Lu10 cells were confirmed with real-time RT-PCR using cDNAs synthesized with the SuperScript III First Strand Synthesis System (Thermo Fisher Scientific, Ltd., Japan). The PCR primer sequences used in this study are shown in Table S1.

Plasmids and stable transfection

The expression vector for mouse S100A14 with enhanced green fluorescent protein (EGFP) was constructed by subcloning a PCR-amplified insert corresponding to the open reading frame of S100A14 into the pEGFP-N1 vector

(Takara Bio). Primer sequences for the expression vector construction were as follows: forward, gaagatcttcaacgatggacagtgtcggt; reverse, tcccccgggggagtagaagtcctcagctccgagtaa. To construct plasmids for S100A14 gene knockdown, predesigned S100A14 miRNA sequences (nt.147–167 and nt. 303–323 in NM_025393.1) or scrambled sequences were generated by Thermo Fisher Scientific. miR RNAi target sequences were as follows: nt147–167 top, TGCTGAATT CTTGGGCATCCTCAGCAGTTTTGGCCACTGACTGAC TGCTGAGGGCCCAAGAATT and bottom, CCTGAATTC TTGGGCCCTCAGCAGTCAGTCAGTGGCCAAAACTGC TGAGGATGCCCAAGAATTC; nt. 303–323 top, TGCTGT TCTCTTCTAACCCACAGTTGGTTTTGGCCACTGACT GACCAACTGTGTTAGAAGAGAA and bottom, CCTGTT CTCTTCTAACACAGTTGGTCAGTCAGTGGCCAA AACCAACTGTGGGTTAGAAGAGAAC. Each miRNA was cloned into the BLOCK-iT Pol II miR RNAi expression vector, according to the manufacturer's instruction. For stable transfection, 66LM and 66HM cells were transfected with the S100A14-pEGFP vectors and S100A14 miR RNAi vectors, respectively, using Lipofectamine 3000 (Thermo Fisher Scientific). Cells were selected with 0.5 mg/ml G418 (Promega, Madison, WA, USA) for 2 weeks and positive clones were further selected by the limiting dilution method.

RNA interference transfection

Three different siRNAs against mouse S100A14 and negative control (RNAi Inc., Japan) were used for transient gene knockdown in vitro. The sequences of the siRNAs are shown in Table S2. For reverse transfection, siRNA duplexes were diluted in 0.1 ml of Opti-MEM I medium to a final concentration of 1 nM in 24-well plates. 1 µl of Lipofectamine MAX reagent (Thermo Fisher Scientific) was added to each well. After 10 min incubation, 0.5 ml of 1×10^5/ml 66HM cells was added to each well in DMEM with 10% FBS. The gene knockdown efficiency of siRNA was determined by real-time quantitative PCR and western blotting with anti S100A14 antibody (Acris Antibodies GmbH, Germany).

Spontaneous metastasis assay

Cultured tumor cells (1×10^7) suspended in 200 µl of PBS were inoculated into the mammary fat pad of 8-week-old female C3H/He mice. At 4 to 6 weeks after inoculation, animals were sacrificed and tumors and major organs were excised. To analyze metastasis macroscopically, we firstly counted the number of metastatic colonies on the whole surface of the lungs and liver and observed the presence of nodules in the ovaries, adrenals and lymph nodes using stereo microscope. To evaluate metastasis microscopically, we prepared lung and liver specimens by cutting each lobe into two pieces after fixation with formaldehyde. We counted the number of colonies in all cut surfaces of the lung under microscope.

In vitro invasion assay

Invasion assays were performed in biocoat cell culture inserts with a polystyrene membrane (8 µm pore; BD Biosciences, San Jose, CA, USA) in a 24-well tissue culture plate. The culture insert was coated with Matrigel (BD Biosciences) at the amount of 8.7 µg/filter. The upper chamber was filled with 1×10^5 cells in culture media with 10% serum. The lower chamber was filled with 700 µl of culture media with 10% serum. After incubation at 37 °C for 24 h, the membranes were removed, stained with hematoxylin, and mounted on slides, and the total cells on the lower side of the membrane were counted under a microscope.

Wound healing assay

66HM cells transfected with S100A14 or control siRNA were seeded on 35 mm plastic dishes until 90% confluent. Cell monolayers were then scratched with a p200 pipette tip and rinsed with culture media. Cells migrating into the scratched region at the same points on the culture dish were recorded using phase-contrast microscopy (Olympus Corp., Japan) at 0 to 24 h. The width of the wound was measured using image analysis and measurement software (SensivMeasure; Mitani Corp., Japan). The extent of cell migration was evaluated as the speed of wound closure for 24 h.

XTT assay

The effect of S100A14 knockdown on in vitro cell growth was examined using the XTT assay kit (BD Biosciences). At 24 h after siRNA transfection, 66HM cells were added with 50 µl XTT labelling mixture containing 2,3-bis-(2-methoxy-4-nitro-5-sulfophenyl)-2H-tetrazolium-5-carboxanilide and phenazine methosulphate (PMS) per well in a 96-well plate. After incubation for 4 h, absorbance at 450 nm was determined using a microtiter plate reader.

Immunofluorescence and western blot analyses

Cultured cells were plated on 8-well chamber slides for 24 to 48 h. Cells were fixed with 4% paraformaldehyde and permeabilized for 5 min at room temperature with 0.1% Triton-X in PBS, followed by blocking for 1 h with 5% skimmed milk. Cells were stained with rabbit polyclonal antibodies for S100A14 (diluted 1/100, Acris), followed by incubation with Alexa Fluor 488-labeled secondary antibody (diluted 1/2000, Molecular Probes, Thermo Fisher), for 1 h at room temperature. Phalloidin conjugated with rhodamine (Cytoskeleton, Inc., Denver, CO, USA)

A Metastatic tumor sublines

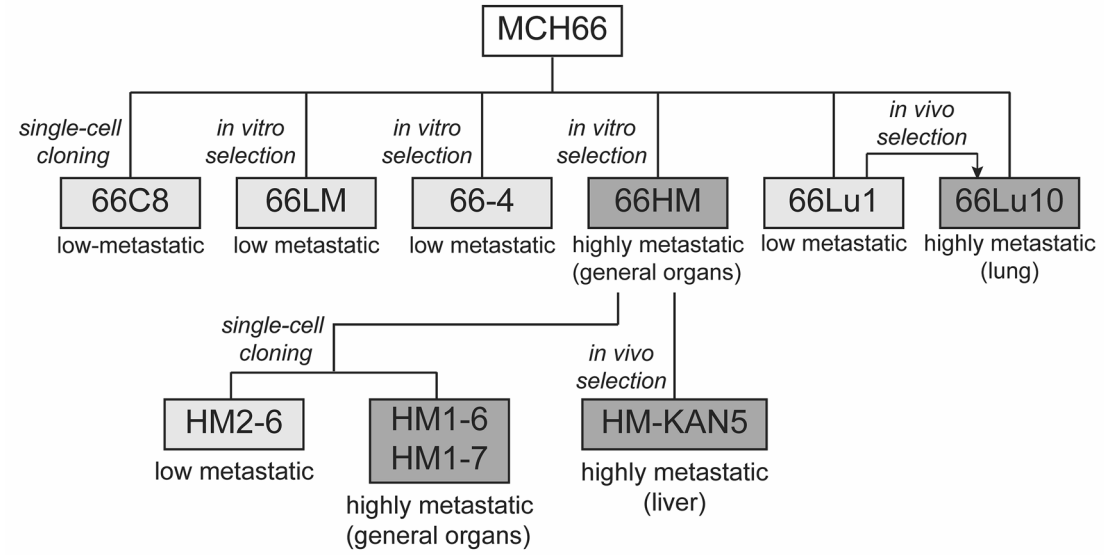

B Spontaneous metastasis assay

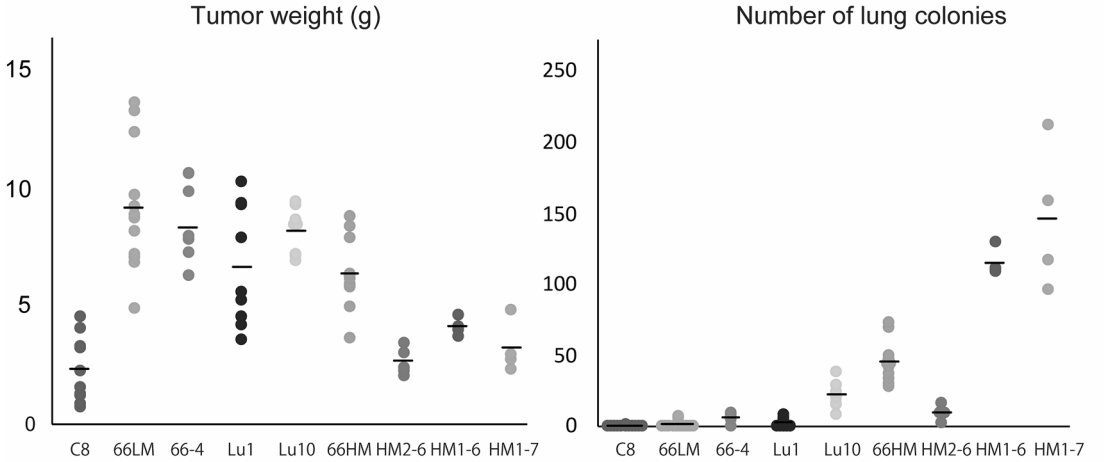

	Tumor weight (g) (at 7 weeks)	Incidence of metastases lung (No. of colonies)	liver (No. of colonies)	lymph node	ovary	adrenal
66C8	2.4	1/12 (0.1)	0/12 (0)	0/12	0/12	0/12
66LM	9.2	2/12 (1.1)	0/12 (0)	0/12	0/12	0/12
66-4	8.3	5/ 6 (6.0)	0/ 6 (0)	0/ 6	0/ 6	0/ 6
66Lu1	6.7	5/10 (2.3)	0/10 (0)	1/10	0/10	0/10
66Lu10	8.2	9/ 9 (21.9)	0/ 9 (0)	9/ 9	0/ 9	0/ 9
66HM	6.4	11/11 (45.6)	5/11 (14.6)	10/11	9/11	3/11
HM2-6	2.7	4/ 4 (12.0)	1/ 5 (0.2)	0/ 5	1/ 5	0/ 5
HM1-6	4.1	4/ 4 (116)	4/ 4 (51.2)	2/ 4	4/ 4	0/ 4
HM1-7	3.2	4/ 4 (147)	4/ 4 (18.5)	3/ 4	2/ 4	3/ 4
66HM*	5.7	5/ 5 (48.2)	3/ 5 (14.6)	5/ 5	4/ 5	2/ 5
HM-KAN5*	2.5	10/10 (54.9)	9/10 (28.1)	0/10	10/10	3/10

◂**Fig. 1** Derivation of metastatic sublines selected from the MCH66 mouse mammary tumor cell line, and their metastatic properties. **a** Dendrogram of sublines. 66C8, 66LM and 66-4 were selected from single cells or several cell clusters in vitro from MCH66 and their low-metastatic activities in vivo were confirmed. 66HM, a highly metastatic subline toward general organs, was generated by in vitro selection. HM2-6, a low-metastatic clone, and HM1-6 and HM1-7, highly metastatic counterparts, were selected by in vitro single-cell cloning method. HM-KAN5, a highly metastatic subline toward the liver, was established by an in vivo selection method. 66Lu10 is an in vivo-selected subline with a highly metastatic capacity to the lung. **b** Tumor weight and the number of macroscopic metastatic nodules in the lung at 7 weeks after orthotopic inoculation of cultured cells into the mammary fat pad. 66HM* and HM-KAN5* in the right and table show data at 6 weeks after tumor cell inoculation, including the number of liver metastatic foci. Horizontal lines in the dot plot indicate group medians

was used for F-actin staining. The slides were mounted in mounting medium containing DAPI and investigated with fluorescence microscopy (Olympus). Western blotting was performed using cellular protein extracted with cell lysis reagent (Sigma-Aldrich Japan, Tokyo, Japan). Equal amounts of proteins were electrophoresed by standard SDS-PAGE under reducing conditions, transferred onto Immobilon membranes (Merck Millipore, Darmstadt, Germany), and the target proteins were detected by immunoblotting according to standard protocols with Amersham ECL Select (GE healthcare Japan, Tokyo, Japan).

Time-lapse imaging

Cells were seeded at 30% confluency on 35 mm dishes. After 24 h, dishes were placed on the stage of an inverted phase-contrast microscope (Olympus) enclosed within an incubator system (Tokai Hit Co. Ltd., Japan). Digital images were obtained with a CCD camera at 10 min intervals for 12 h.

Immunohistochemical analysis

Immunostaining was performed using an indirect streptavidin–biotin immunoperoxidase method (SAB-PO (M) kit; Nichirei Corp., Japan). After antigen retrieval in a microwave oven for 15 min in 10 mM citrate buffer, pH 6.0, endogenous peroxidase activity was blocked with a 3% H_2O_2-methanol solution. The slides were incubated with primary antibodies of S100A14 (diluted 1/1000), overnight at 4 °C, washed with PBS, and then incubated with secondary biotin-labelled antibodies (diluted 1/50,000), for 30 min at room temperature. Antibody localization was visualized with peroxidase-conjugated streptavidin for 30 min at room temperature, followed by the diaminobenzidine reaction. The slides were counterstained with hematoxylin.

Statistical analysis

In general, most data represent the mean ± SD and are representative of four independent experiments, except for in vivo tumor growth, and metastasis experiments. To test for significant differences between two groups, unpaired Student *t* tests were used. Two-sided p values < 0.05 were considered significant. These analyses were carried out using SPSS v.19.0.

Results

Establishment of murine metastasis model

To explore the molecular mechanism of cancer metastasis, we established various sublines differing in metastatic activity, pathway and organotropism from a mouse mammary tumor cell line, MCH66, which originally exhibited metastatic potential to the lung through an invasion-independent pathway. The sublines in this model system are shown in Fig. 1a.

66C8 is the only non-metastatic clone that we could select by single cell cloning from MCH66 [2]. However, single cell cloning was technically difficult and seemed unnatural as a selection method because most cells of MCH66 were highly cohesive. Then, we used an alternative method, in which clusters of 5 to 10 tumor cells were isolated by limiting dilution. After confluent growth in a 96-well plate, we selected a colony consisting of tumor cells with uniform morphology under an inverted microscope and examined its metastatic potential in vivo. Using this method, we established low-metastatic sublines, 66LM and 66-4, and a highly metastatic subline, 66HM. In addition, we selected a low-metastatic clone, HM2-6, and two highly metastatic clones, HM1-6 and HM1-7, by single cell cloning from 66HM. The morphologies of cultured sublines are shown in Supporting Information, Fig. S1.

To select cell populations with enhanced metastatic capability for specific organs, metastatic colonies in the lung or liver after orthotopic inoculation in the mammary fat pad was isolated and cultured. Cultured cells were harvested and inoculated into the fat pad of another set of syngeneic mice. After ten or five selection cycles, we established two sublines, 66Lu10 [6] from MCH66 and HM-KAN5 from 66HM, which have organotropic metastasis capacity for the lung and liver, respectively.

Spontaneous metastatic activity for each subline is shown in Fig. 1b. In the 66Lu series, 66Lu10 formed a much higher number of lung metastatic colonies than 66Lu1, a subline obtained after only one selection cycle. In the HM-KAN series, HM-KAN5 had many macroscopic colonies in the liver at 6 weeks after inoculation, whereas the tumor weight

was the least of the series. In addition, at 4 weeks, HM-KAN5 already formed microscopic foci of liver metastasis at a higher number than the parent cell line, 66HM, and the series of HM-KAN1 to HM-KAN4 (Supporting Information Fig. S2).

As a result, we established a series of low-metastatic sublines: 66C8, 66LM, 66-4, HM2-6 and 66Lu1, and highly metastatic sublines: 66HM, HM1-6, HM1-7, 66Lu10 and HM-KAN5, from MCH66 mouse mammary tumor cells. All of the highly metastatic sublines yielded spontaneous lung metastasis with a higher incidence and a higher number of metastatic colonies, while the series of 66HM sublines disseminated to multiple organs: adrenals, ovaries, liver and lymph nodes, and lungs (Fig. 1b).

These metastatic sublines utilized the invasion-independent pathway of blood-borne metastasis, which is characterized by the induction of well-developed sinusoidal tumor vessels in the primary tumor, intravasation of multicellular tumor clusters enveloped by vascular endothelial cells and intravascular tumor growth embolized in pulmonary arteries (Fig. 2Aa–c). In contrast, the 66HM series produced smaller tumor cell emboli without endothelial covering and were observed within capillary vessels in the kidney and liver (Fig. 2Ad), suggesting the coexistence of an alternative pathway different from the invasion independent pathway.

The XTT assay revealed no differences in in vitro growth properties among the sublines (Fig. 2B). Invasive activities

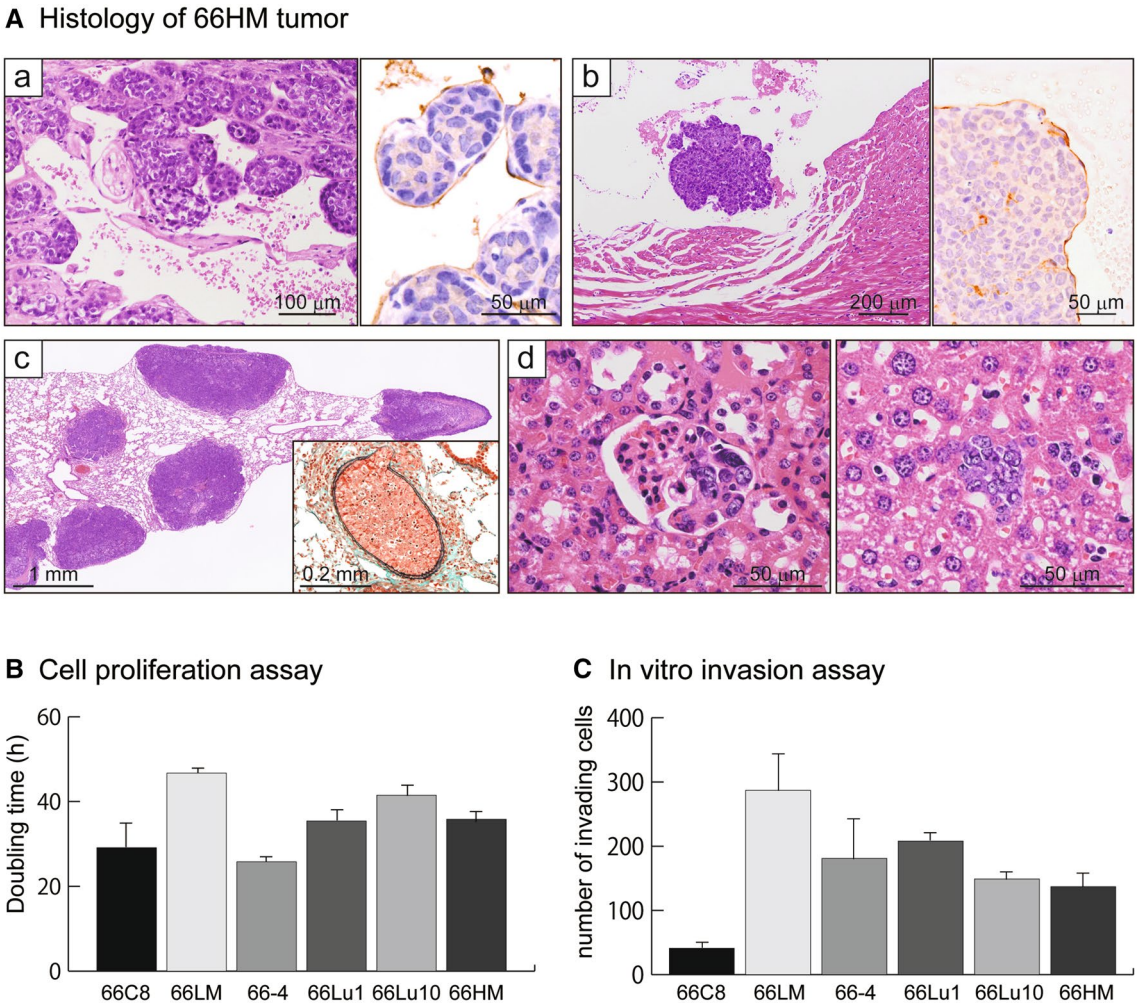

Fig. 2 Morphologies and cell properties of the sublines selected from the MCH66 cell line. **A** Representative histologic features of 66HM, a highly metastatic subline. The primary tumor formed well-developed sinusoidal tumor vasculature, which entirely enveloped tumor nests (a, left). Immunohistochemistry using CD34 antibody shows endothelial wrapping on the tumor nests (a, right). The tumor emboli covered by endothelial cells were found within the right cardiac ventricle (b). Multiple metastatic nodules in the lung contained expanded arteriole filled with embolized tumor cells (c). The emboli of 66HM in the kidney (d, left) and liver (d, right) formed small clusters with no accompanying endothelial cells. **B** In vitro growth property of the sublines assessed by the XTT assay. Error bars, ± SD (n = 3). **C** Invasive activity of the sublines assessed by in vitro invasion assay using Matrigel-coated membranes. Error bars, ± SEM (n = 3)

of the sublines did not correspond with their metastatic potentials (Fig. 2C).

Comprehensive screening of metastasis-associated genes

To identify genes with potential involvement in metastasis, we initially selected genes that were differentially expressed genes between highly metastatic sublines and their lower metastatic counterparts in three sets (66HM to 66LM, HM1-6 to HM2-6 and HM1-7 to HM2-6) using DNA microarray analysis. In addition, we extracted candidate genes for organotropic metastasis to the lung and liver by comparing 66Lu10 to 66Lu1 using suppressive subtractive hybridization (SSH) and HM-KAN3 or HM-KAN5 to 66HM using DNA microarray analysis.

The major candidates of metastasis-promoting genes, which are expressed at levels of more than fourfold higher in highly metastatic sublines relative to low-metastatic counterparts, are shown in Supplementary Table 2. To focus on more promising candidates that promote metastasis, we combined two sets of data (66Lu10 to 66Lu1 and 66HM to 66LM) and extracted 44 genes that were commonly overexpressed in both sets. In addition, we confirmed the expressions of the candidate genes using real-time quantitative RT-PCR method in five sublines, including the non-metastatic line 66C8. Consequently, 19 genes were selected as metastasis-promoting candidate genes (Table 1). Of these 19 genes, we focused on the top 5 genes; *S100A14, Hey1, Col9a, SEMA3B and EMID1*, which were expressed especially high in 66HM, a subline with highly metastatic potential to the general organs and we proceeded to the following studies, including a metastatic assay and analyses of the molecular functions using transfection and knockdown methods of the target genes. *S100A14* was one of these most promising candidates. Real-time RT-PCR confirmed that *S100A14* mRNA expression correspond to the metastatic potential of sublines derived from MCH66 (Fig. 3a). Immunohistochemistry revealed that S100A14 protein was diffusely expressed on the cell membrane of highly metastatic cells.

S100A14 promotes tumor cell scattering and metastasis

To investigate the association of S100A14 expression with metastasis, we transfected low-metastatic subline, (66LM and 66-4) with an expression vector encoding S100A14 to obtain stably overexpressing transfectants. We then selected two clones (66-4 A14-1 and 66-4 A14-2) that maintained high expression levels in vivo (Fig. 3b). The inoculated tumors produced with these transfectants showed a drastic morphological change in the scattering of spindle-shaped tumor cells at the invasion front, whereas 66-4 cells

Table 1 Metastasis-promoting candidate genes reevaluated by real-time RT-PCR

No.	Symbol	Gene name	Relative mRNA expression		
			HM/LM	HM/C8	Lu10/Lu1
50	**S100A14**	**S100A14**	**12.5**	**14.0**	**2.2**
13	Hey1	Hairy/enhancer-of-split related with YRPW motif 1	66.7	18.0	4.3
42	Col9a1	Procollagen, type IX, alpha 1	107.5	4.0	2.0
32	Col9a2	Collagen, type IX, alpha 2	56.4	11.0	5.1
5	SEMA3B	SEMAPHORIN 3B	44.0	2.2	3.4
47	Emid1	EMI domain containing 1	18.8	5.9	1.6
2	Med24	Mediator complex subunit 24	6.6	1.4	3.4
4	Ltbp2	Latent TGF-beta binding protein-2	6.2	3.7	2.1
6	Fhdc1	FH2 domain containing 1	4.0	3.5	10.0
46	Stac2	SH3 and cysteine rich domain 2	3.8	0.9	2.2
44	Pygb	Brain glycogen phosphorylase	3.6	2.4	4.4
53	Fgfrl1	Fibroblast growth factor receptor-like 1	3.5	12.0	10.4
61	Tesc	Tescalcin	3.5	4.3	1.6
1		EST	3.2	14.0	4.4
60	Iqgap1	IQ motif containing GTPase activating protein 1	3.1	1.3	1.5
27	Ppfibp2	PTPRF interacting protein, binding protein 2	2.6	39.0	4.2
23	Yars	Tyrosyl-tRNA synthetase	2.2	4.4	3.9
36	Pml	Promyelocytic leukemia	2.2	2.6	4.3
30	Mgea5	Meningioma expressed antigen 5	2.0	4.9	3.4

Bold means the gene that we focused on this study

HM 66HM, *LM* 66LM, *C8* 66C8, *Lu10* 66Lu10, *Lu1* 66Lu1

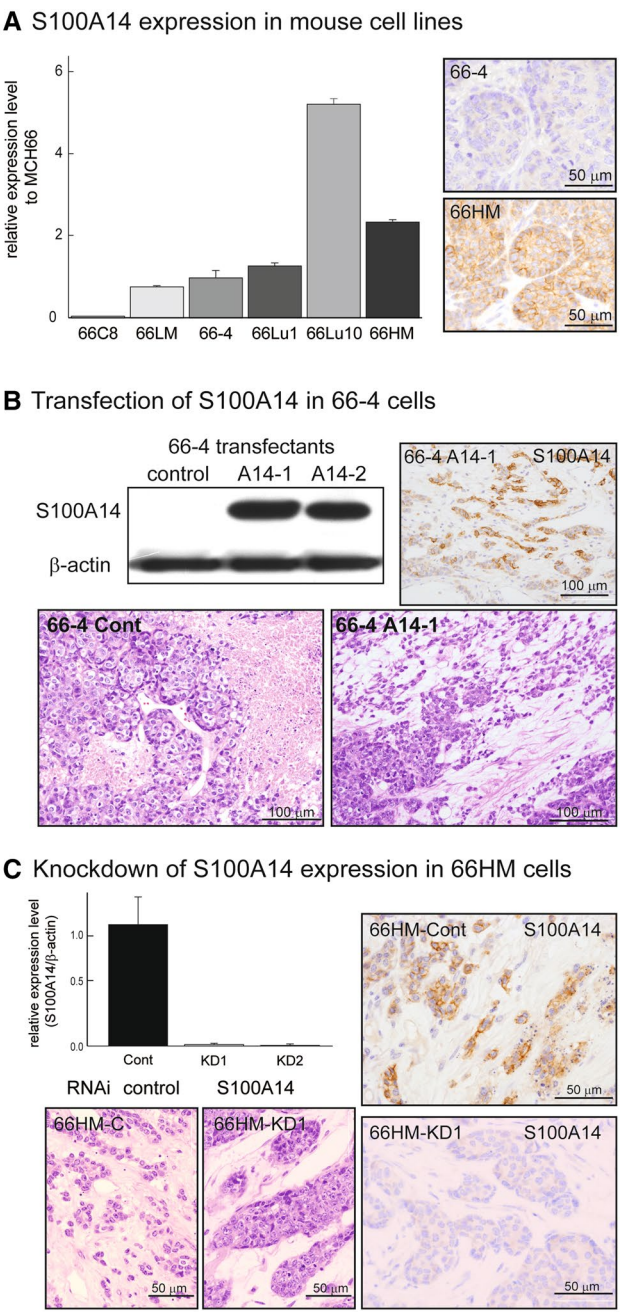

Fig. 3 Effect of S100A14 expression on in vivo tumor morphology of mouse mammary tumor cells. **a** S100A14 mRNA expression in vitro measured by real-time qRT-PCR (left). Error bars, ±SEM (n = 3). Representative immunohistochemical images of S100A14 protein expression in vivo (right). S100A14 protein is localized in the plasma membrane of 66HM cells. **b** Morphological change of 66-4 cells, a low-metastatic subline, induced by S100A14 overexpression. 66-4 cells transfected with S100A14 expression vector, 66-4 A14-1 and A14-2, overexpressed S100A14 protein, which was detected by western blotting of cultured cells (top left) and immunohistochemistry of the inoculated tumor (top right). Overexpression of S100A14 induced scattering of 66-4 cells, whereas 66-4 cells transfected with control vector remained cohesive in vivo (bottom). **c** Morphological changes in 66HM cells following stable knockdown of S100A14 expression. Stable transfection of miRNA vectors targeting different sequences (KD1 and KD2) reduced S100A14 expressions at both the mRNA level (qRT-PCR, top left) and the protein level (immunohistochemistry, right), compared with 66HM-Cont transfected with the control vector. Error bars, ±SEM (n = 3). Knockdown of S100A14 enhanced cohesiveness of 66HM cells to form tumor nests, whereas 66HM-Cont maintained cell scattering (bottom left)

transfected with a control vector maintained a nested formation of cohesive tumor cells (Fig. 3b). Overexpression of S100A14, however, did not increase either tumor weight or spontaneous metastasis of the low-metastatic cells (data not shown). Next, we established stable knockdown of *S100A14* gene expression using transfection of miRNA expression vector in the highly metastatic subline 66HM and selected the lowest-expressing cell clones: HM-KD1 and HM-KD2, by the single-cell cloning method (Fig. 3c). In the in vivo experiment, both HM-KD1 and HM-KD2 reduced cell scattering and formed solid tumor nests, whereas the mock transfectants of 66HM maintained the scattering feature like 66HM cells. At 5 weeks after orthotopic inoculation, the knockdown cells significantly decreased the number of metastatic colonies in the lung compared with control cells ($p < 0.01$), whereas tumor weight did not show a significant difference (Fig. 4). These data indicate that S100A14 functions to promote cell scattering in vivo and spontaneous metastasis.

Knockdown of S100A14 suppresses cell motility and invasive activity in vitro

To determine the functional role of S100A14 protein in mouse mammary tumor metastasis, we performed in vitro studies on several factors in the metastatic process (cell proliferation, motility and invasion) using siRNA against mouse *S100A14* in 66HM cells. We prepared three different siRNA target sequences (siA14-1, 2 and 3) to ensure the specificity of the knockdown effect.

Real-time PCR analysis revealed that siA14-2 and siA14-3 suppressed S100A14 expression to the greatest extent (Fig. 5a), and siA14-2 was selected for use in the subsequent knockdown studies. First, we examined the effect of S100A14 knockdown on the in vitro proliferation of 66HM cells using the XTT assay system. There was no significant difference between the transfectants with siRNA for S100A14 and control siRNA (Fig. 5b). Next, we determined the migration/invasion activity using two assay systems, the in vitro invasion assay and the wound-healing assay. 66HM cells transfected with siRNA for S100A14 significantly reduced migration activity through Matrigel compared with control siRNA transfectants (Fig. 5c). The wound healing assay also revealed that knockdown of S100A14 suppressed cell motility (Fig. 5d).

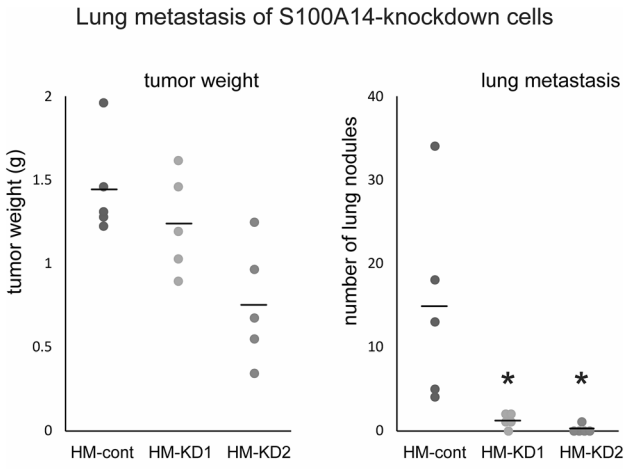

	tumor weight (g)	lung metastasis (number of colonies)
HM-Cont	1.45	14.8
HM-KD1	1.24	1.2
HM-KD2	0.75	0.2

Fig. 4 Effect of stable knockdown of S100A14 on the spontaneous metastasis of the 66HM subline. 66HM stably transfected with miR RNA expression vectors, HM-KD1 and HM-KD2, significantly reduced the number of lung metastatic nodules ($p < 0.01$) compared with mock transfectant, HM-Cont. However, there were no significant differences in tumor weight between HM-Cont and HM-KD1 or HM-KD2. Horizontal lines indicate group medians

Furthermore, knockdown of S100A14 induced morphological changes of the cultured cells. Under a subconfluent condition, 66HM transfected with control siRNA exhibited polygonal morphology with multiple processes, whereas S100A14-knockdown cells exhibited increased cell–cell contact, forming cohesive cell islands (Fig. 5e). Time-lapse video microscopy showed suppression of cell motility by knockdown of S100A14 in 66-HM cells (Supporting Information Videos S1 and S2). Furthermore, filamentous formation of F-actin in 66HM cells was inhibited by knockdown of S100A14 (Fig. 5e).

Discussion

The aims of this study are to establish suitable models for the various types of cancer metastasis and elucidate the molecular mechanism involved in metastasis formation for each type using these models. We established multiple sublines originating from the mouse mammary tumor cell line, MCH66, with different metastatic abilities, organotropism and metastasis pathways using a variety of selection methods, including in vitro cell cloning and in vivo selection of metastatic cells. Using this model, we identified S100A14 as a candidate metastasis-promoting molecule through comprehensive gene expression analysis.

MCH66 was derived from a mammary tumor spontaneously developed in C3H mice and appeared to be a heterogeneous cell line containing various subpopulations; thus, we were able to isolate many sublines with different metastatic properties according to various selection pressures. One of the features of this model is that it consists of several pairs of highly and low-metastasis: 66Lu1 to 66Lu10, 66HM to HM-KAN5 and HM2-6 to HM1-6 or HM1-7, enabling the easy comparison of events and molecules involved in metastasis.

This model system also includes sublines with various organotropic metastasis. 66Lu10 shows high metastatic activity to the lung [6], and HM-KAN5 has a predilection for metastasis to the liver. In contrast, 66HM is a highly metastatic subline that can disseminate to the general organs including lung, liver and lymph nodes. Furthermore, of the clones selected from 66HM, HM1-6 and HM1-7 exhibited enhanced metastatic properties, whereas HM 2-6 showed attenuated metastatic activity.

In addition, this system includes two different models of metastasis pathways. The parent line, MCH66, utilizes the invasion-independent metastasis pathway, which is characterized by multicellular tumor emboli covered by vascular endothelial cells [2], while the 66Lu10 seems to enhance this pathway [6]. On the other hand, the sublines in the HM series: 66HM, HM1-6, HM2-7 and HM-KAN5, yield smaller-sized naked emboli in microvessels of the target organs as well as endothelilalized emboli in the cardiac ventricle, suggesting the coexistence of a pathway dependent on invasive activity of tumor cells in the intravasation step.

Using this model system, we examined the representative biological properties involved in metastasis. Growth and invasion properties in vitro were not necessarily correlated with metastatic potential; for example, both properties of the low-metastatic subline 66LM were higher than those of all other highly metastatic sublines. These data may not be surprising because metastasis of this model is based on the invasion-independent pathway. However, in vitro assays may not necessarily reflect the global events of metastasis in vivo, which require different cellular activities such as proliferation, survival, adhesion/detachment, motility, invasion, etc., in each step.

In a comprehensive and comparative analysis of gene expression between low- and highly metastatic sublines, metastasis-related gene candidates were extracted in each pair (Supplementary Table 2) and 19 genes common to multiple combinations were identified as promising candidates for metastasis-promoting genes (Table 1). In fact, we have confirmed that some of the gene candidates can promote metastatic activity in an in vivo metastasis assay using overexpression or knockdown experiments (data not

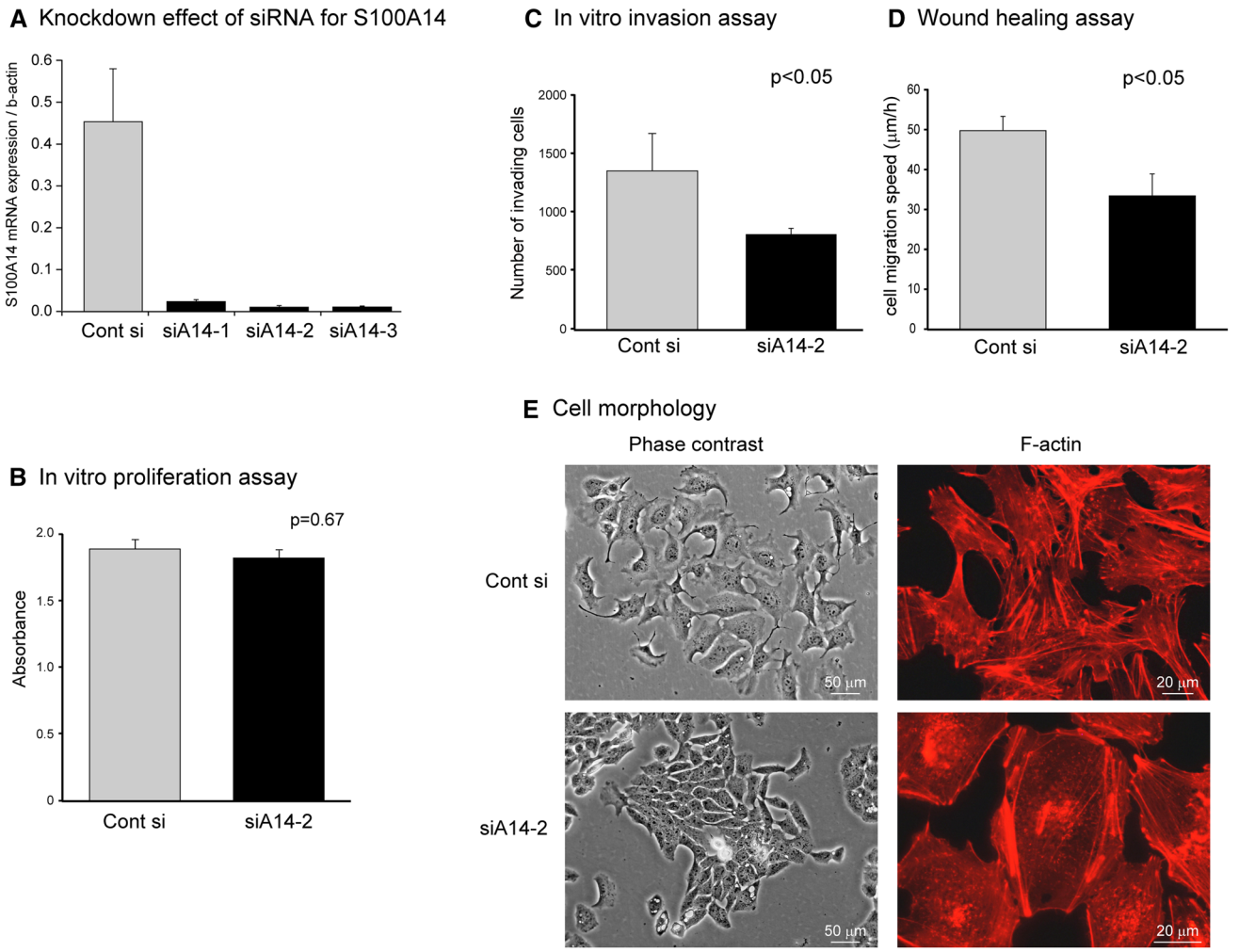

Fig. 5 Effects of transient knockdown of S100A14 on in vitro properties of the 66HM subline. **a** Significant reduction of S100A14 mRNA expressions by transfection of specific siRNAs targeting three different sequences (siA14-1, siA14-2, and siA14-3) were confirmed by quantitative qRT-PCR. Control siRNA was used as nonsilencing siRNA. The data presented in (**b**–**e**) were obtained using siA14-2. **b** Cell proliferation was quantified by XTT assay at 48 h after transfection with the siRNAs. **c** In vitro invasion assay using Matrigel. At 24 h after transfection with the siRNAs, 1×10^5 cells were seeded on the culture insert with an 8 μm pore membrane coated with Matrigel. After 24 h incubation, the number of migrated cells was counted. **d** Cell motility was analyzed by wound healing assay. After scratching the cell monolayers, the speed of wound closure for 24 h was calculated. **e** Morphological change induced by S100A14 knockdown in 66HM. Cells were imaged using phase contrast and immunofluorescence with phalloidin conjugated with rhodamine for F-actin staining. All error bars, ± SEM (n = 3)

shown). In this analysis, we also extracted several candidates for metastasis-suppressing genes (data not shown).

Among the 19 genes identified here, S100A14 is one of the most promising candidate genes for promoting metastasis. In fact, knockdown of S100A14 significantly suppressed lung metastasis in the high-expressors, whereas overexpression of this gene did not enhance the metastatic potential in the low-expressors (data not shown). These results seem to be contradictory. However, metastatic process involves multiple steps and molecules. Presumably these data show that S100A14 may be one of the essential molecules for metastasis but does not act alone to drive metastasis. Our model will enable the identification of concomitant, necessary genes for metastasis competency.

Our in vivo and in vitro experiments suggest that S100A14 can promote invasion and metastasis via cell scattering and motility. In our previous study using human breast cancer cells, we showed that S100A14 protein can bind to cortical actin to promote cell motility via an interaction with cytoskeletal dynamics [7]. High expression of S100A14 has also been reported to promote motility and invasiveness of cancers of the lung, uterine cervix, ovary and breast [17–21]. In contrast, there are some reports indicating that S100A14 expression suppresses invasion of gastric, urothelial, and

oral squamous cell carcinomas [16, 22, 23]. Members of the S100 protein family, to which S100A14 belongs, are known to be multifunctional proteins that bind to a variety of other proteins to modify their intracellular functions [8, 9]. In fact, several proteins such as actin, HER2 and RAGE have been identified as target proteins for S100A14 binding [7, 10, 11]. The conflicting effects of S100A14 on motility and invasion may depend on the target proteins of S100A14 in each cancer type.

Since all sublines in our model system are derived from the MCH66 cell line, which has a metastatic potential via the invasion-independent pathway, the conclusion that S100A14 promotes metastasis by enhancing invasiveness appears to be contradictory in this system. However, our concept of the invasion-independent metastasis pathway implies a mechanism by which cancer cells can intravasate without destroying the vascular wall, so that it does not deny the involvement of invasion in other steps of the metastasis process [24]. Furthermore, the highly metastatic subline 66HM, in which S100A14 knockdown successfully suppressed metastatic activity in this study, showed not only the "invasion-independent pathway" but also the "invasion-dependent pathway", featuring naked tumor cell emboli within capillaries of the target organs. The suppression of metastasis in this experiment might be due to inhibition of the latter pathway.

The purpose of establishing this mouse model is to elucidate the various metastasis mechanisms in human cancer and its application to clinical practice. We are conducting clinicopathological analysis of several candidate metastasis-related molecules identified in this study. For S100A14, we have reported that high expression of this protein correlates with poor prognosis of breast cancer patients, indicating that this molecule represents a possible biomarker for breast cancer [7]. For other candidate molecules, we are now conducting a multistage study comprised of verification of the metastasis-promoting effect using in vivo assays, analysis of molecular functions using mouse and human cancer cell lines and correlation analysis with prognostic factors of cancer patients. Our metastasis model may be useful for elucidation of the molecular mechanism of cancer metastasis and screening of target molecules for prognostic prediction and therapy of cancer patients.

Author contributions The authors contributed as follows: TS, NIT, MT and NS: were involved in the study concept and experimental design; TS, NS, TM, MA and KM: performed molecular and animal experiments; TO, YK and TK: helped with the analysis and interpretation of data (statistical analysis, biostatistics, computational analysis); YA: supervised the whole process. TS and NS: wrote the manuscript. All authors read and approved the final manuscript.

Funding This work was supported by a Grant-in-Aid for Scientific Research (C) from the Japan Society for the Promotion of Science (16K08727).

Data availability All data generated or analyzed during this study are included in this published article.

Compliance with ethical standards

Conflict of interest The authors declare that they have no conflict of interest.

Ethics approval All animal studies were carried out under the control of the Animal Care and Use Committee in accordance with the Guidelines for Animal Experiments of Fukushima Medical University and Shizuoka Cancer Center.

References

1. Naxerova K, Reiter JG, Brachtel E, Lennerz JK, van de Wetering M, Rowan A et al (2017) Origins of lymphatic and distant metastases in human colorectal cancer. Science (New York, NY) 357:55–60
2. Sugino T, Kusakabe T, Hoshi N, Yamaguchi T, Kawaguchi T, Goodison S et al (2002) An invasion-independent pathway of blood-borne metastasis: a new murine mammary tumor model. Am J Pathol 160:1973–1980
3. Sugino T, Yamaguchi T, Hoshi N, Kusakabe T, Ogura G, Goodison S et al (2008) Sinusoidal tumor angiogenesis is a key component in hepatocellular carcinoma metastasis. Clin Exp Metastasis 25:835–841
4. Sugino T, Yamaguchi T, Ogura G, Saito A, Hashimoto T, Hoshi N et al (2004) Morphological evidence for an invasion-independent metastasis pathway exists in multiple human cancers. BMC Med 2:9
5. Sugino T, Yamaguchi T, Ogura G, Kusakabe T, Goodison S, Homma Y et al (2007) The secretory leukocyte protease inhibitor (SLPI) suppresses cancer cell invasion but promotes blood-borne metastasis via an invasion-independent pathway. J Pathol 212:152–160
6. Ogura G, Sugino T, Suzuki T, Nakamura N (2014) Establishment of highly metastatic cell line (Lu10) from murine mammary carcinoma cell line MCH66 and biological characteristics of Lu10. Tokai J Exp Clin Med 39:72–79
7. Tanaka M, Ichikawa-Tomikawa N, Shishito N, Nishiura K, Miura T, Hozumi A et al (2015) Co-expression of S100A14 and S100A16 correlates with a poor prognosis in human breast cancer and promotes cancer cell invasion. BMC Cancer 15:53
8. Chen H, Xu C, Jin Q, Liu Z (2014) S100 protein family in human cancer. Am J Cancer Res 4:89–115
9. Santamaria-Kisiel L, Rintala-Dempsey AC, Shaw GS (2006) Calcium-dependent and -independent interactions of the S100 protein family. Biochem J 396:201–214
10. Xu C, Chen H, Wang X, Gao J, Che Y, Li Y et al (2014) S100A14, a member of the EF-hand calcium-binding proteins, is overexpressed in breast cancer and acts as a modulator of HER2 signaling. J Biol Chem 289:827–837
11. Jin Q, Chen H, Luo A, Ding F, Liu Z (2011) S100A14 stimulates cell proliferation and induces cell apoptosis at different concentrations via receptor for advanced glycation end products (RAGE). PLoS ONE 6:e19375
12. Ehmsen S, Hansen LT, Bak M, Brasch-Andersen C, Ditzel HJ, Leth-Larsen R (2015) S100A14 is a novel independent prognostic biomarker in the triple-negative breast cancer subtype. Int J Cancer 137:2093–2103

13. Qian J, Ding F, Luo A, Liu Z, Cui Z (2016) Overexpression of S100A14 in human serous ovarian carcinoma. Oncol Lett 11:1113–1119
14. Kim G, Chung JY, Jun SY, Eom DW, Bae YK, Jang KT et al (2013) Loss of S100A14 expression is associated with the progression of adenocarcinomas of the small intestine. Pathobiology 80:95–101
15. Zhao H, Guo E, Hu T, Sun Q, Wu J, Lin X et al (2016) KCNN4 and S100A14 act as predictors of recurrence in optimally debulked patients with serous ovarian cancer. Oncotarget 7:43924–43938
16. Zhu M, Wang H, Cui J, Li W, An G, Pan Y et al (2017) Calcium-binding protein S100A14 induces differentiation and suppresses metastasis in gastric cancer. Cell Death Dis 8:e2938
17. Katono K, Sato Y, Kobayashi M, Saito K, Nagashio R, Ryuge S et al (2017) Clinicopathological significance of S100A14 expression in lung adenocarcinoma. Oncol Res Treat 40:594–602
18. Wang X, Yang J, Qian J, Liu Z, Chen H, Cui Z (2015) S100A14, a mediator of epithelial-mesenchymal transition, regulates proliferation, migration and invasion of human cervical cancer cells. Am J Cancer Res 5:1484–1495
19. Cho H, Shin HY, Kim S, Kim JS, Chung JY, Chung EJ et al (2014) The role of S100A14 in epithelial ovarian tumors. Oncotarget 5:3482–3496
20. He H, Li S, Chen H, Li L, Xu C, Ding F et al (2014) 12-O-tetradecanoylphorbol-13-acetate promotes breast cancer cell motility by increasing S100A14 level in a Kruppel-like transcription factor 4 (KLF4)-dependent manner. J Biol Chem 289:9089–9099
21. Chen H, Yuan Y, Zhang C, Luo A, Ding F, Ma J et al (2012) Involvement of S100A14 protein in cell invasion by affecting expression and function of matrix metalloproteinase (MMP)-2 via p53-dependent transcriptional regulation. J Biol Chem 287:17109–17119
22. Lee MS, Hsu WT, Deng YF, Lin CW, Weng EY, Chang HP et al (2016) SOX2 suppresses the mobility of urothelial carcinoma by promoting the expression of S100A14. Biochem Biophys Rep 7:230–239
23. Sapkota D, Bruland O, Costea DE, Haugen H, Vasstrand EN, Ibrahim SO (2011) S100A14 regulates the invasive potential of oral squamous cell carcinoma derived cell-lines in vitro by modulating expression of matrix metalloproteinases, MMP1 and MMP9. Eur J Cancer 47:600–610
24. Sugino T, Kawaguchi T, Suzuki T (1993) Sequential process of blood-borne lung metastases of spontaneous mammary carcinoma in C3H mice. Int J Cancer 55:141–147